Received: 25 August 2025 | Revised: 9 October 2025 | Accepted: 10 November 2025

https://doi.org/10.1016/j.rpth.2025.103274

ORIGINAL ARTICLE

Red blood cell–derived transglutaminase 2 influences thrombus formation

Naoual Ouazzani Chahdi[1] | Judith J. de Vries[2] | Hande Eyisoylu[2,3] | Hanke L. Matlung[1] | Chi Hau[4,5] | Rienk Nieuwland[4,5] | Moniek P. M. de Maat[2] | Joost C. M. Meijers[6,7] | Robin van Bruggen[1]

[1]Sanquin Research and Landsteiner Laboratory, Amsterdam, Amsterdam, Netherlands

[2]Department of Hematology, Cardiovascular Institute, Erasmus MC, University Medical Center Rotterdam, Rotterdam, Netherlands

[3]Department of Bionanoscience, Kavli Institute of Nanoscience, Delft University of Technology, Delft, Netherlands

[4]Amsterdam UMC, University of Amsterdam, Laboratory of Experimental Clinical Chemistry, Laboratory Specialized Diagnostics & Research, Department of Laboratory Medicine, Amsterdam, Netherlands

[5]Amsterdam Vesicle Center, Amsterdam University Medical Centers, Location AMC, Amsterdam, Netherlands

[6]Department of Experimental Vascular Medicine, Amsterdam UMC, University of Amsterdam, Netherlands

[7]Synapse Research Institute, Maastricht, Netherlands

Correspondence
Robin van Bruggen, Sanquin Research, Department of Molecular Hematology Plesmanlaan 125, 1066CX, Amsterdam, Netherlands.
Email: r.vanbruggen@sanquin.nl

Handling Editor: Dr Robert A. Campbell

Abstract

Background: Red blood cells (RBCs) are important constituents of venous clots and contribute to thrombus size and stability. However, it remains unclear whether and how RBCs affect the thrombus. Transglutaminase (TG)2), a protein with similar activity to factor XIIIa, may influence thrombus characteristics.

Objectives: We explored whether RBC-derived TG2 influences thrombus characteristics using a novel approach involving TG2 knockout (KO) RBCs.

Methods: Inhibitors and TG2 KO RBCs were used in clotting assays. *In vitro*–generated clots were analyzed using advanced microscopy techniques to quantify the fibrin network. Whole blood clotting kinetics were assessed by thrombin generation assay and thromboelastography. Vesiculation was assessed using microparticle flow cytometry.

Results: Our study showed clots formed with TG2 KO RBCs or upon TG2 inhibition displayed fewer and thinner fibrin fibers at the clot surface. Inhibition of TG2 further revealed a redistribution of fibrin away from the clot surface toward deeper regions. Functionally, TG2 inhibition accelerated thrombin generation and clot formation, as shown by shortened lag time in thrombin generation assay and faster kinetics in thromboelastography. A normal fibrin density was observed in clots treated with the TG2 inhibitor after addition of RBC-derived extracellular vesicles (EVs). Moreover, TG2 inhibition increased EV formation, associated with more phosphatidylserine exposure on RBC membranes.

Conclusion: TG2 activity within RBCs plays a specific role in modulating EV formation, which in turn influences the fibrin structure and spatial distribution within blood clots. Absence of TG2 activity leads to more EV formation, promoting faster thrombin generation and clot formation, suggesting a regulatory role for TG2 in coagulation kinetics.

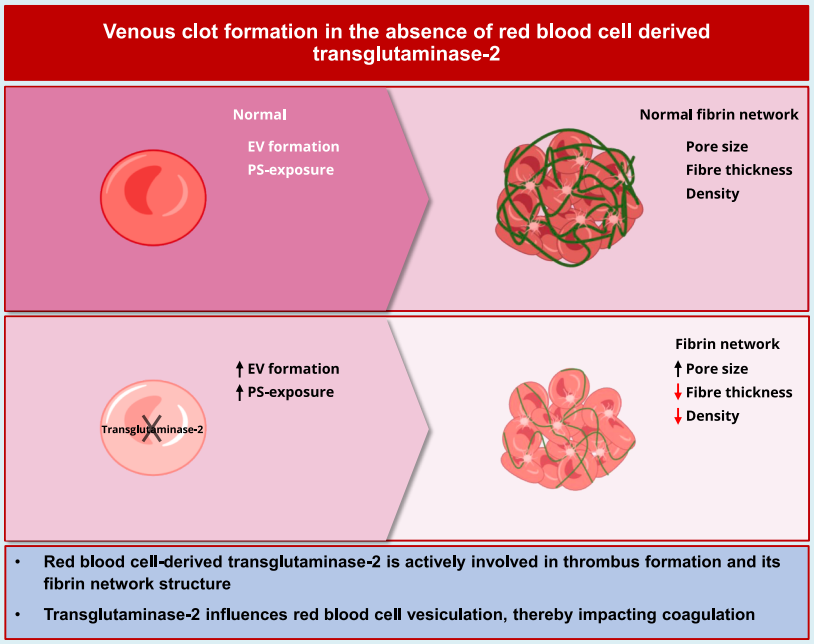

KEYWORDS
extracellular vesicles, fibrin, red blood cells, transglutaminase 2, venous thrombosis

Essentials

- We examined the role of TG2 expressed by RBCs in clotting.
- We used inhibitors as well as gene-edited RBCs to study the role of RBC-derived TG2 in clotting.
- TG2 activity modulates EV formation in RBC, which influences thrombin generation.
- Loss of TG2 function or expression in RBCs changes the structure of the fibrin network.

1 | INTRODUCTION

Hemostasis is essential for preventing blood leakage from damaged vessels, but disturbances can cause bleeding or thrombosis. Thrombosis is a vascular event that involves undesired clotting of blood within vessels resulting in an obstruction in the veins or arteries. Upon vessel damage, platelets adhere and aggregate to form a platelet plug (primary hemostasis), which is then strengthened by the formation of the fibrin network (secondary hemostasis) [1]. The formation of the fibrin network is initiated by the coagulation cascade, leading to the formation of thrombin, which is the central enzyme of the coagulation cascade and responsible for the conversion of fibrinogen into fibrin [2,3].

The overall pathophysiology of venous thromboembolism (VTE) is still incompletely understood, and VTE remains a life-threatening disease that affects 1 to 2 individuals per 1000 adults annually [4,5]. Most studies focus on the role of platelets and coagulation factors [6–10]. Despite the fact that a venous clot mainly consists of red blood cells (RBCs), only limited research has been conducted on the role of RBCs in VTE pathology. RBCs reduce thrombus permeability [11] and increase resistance to fibrinolysis [12]. For a long time, RBCs were viewed as innocent bystanders in the clotting process. Nonetheless, a steadily increasing body of evidence suggests a more complicated relationship between RBCs and thrombosis [13–18]. For example, RBCs contribute to the size of a thrombus. In addition, there is an increased risk of thrombosis after RBC transfusion [19,20].

Coagulation factor (F)XIII(a), a member of the transglutaminase family, functions as a clot stabilizing factor by crosslinking α- and γ-chains of fibrin monomers during thrombus formation [21]. RBCs express high levels of transglutaminase (TG)2, a protein with an activity highly homologous to FXIIIa, as it can also mediate protein crosslinking via transamidation [22]. It is established that TG2 contributes to the preservation and stabilization of the RBC membrane skeleton by catalyzing crosslinking reactions among fundamental membrane proteins, including spectrin, actin, ankyrin, and band 3 [23]. In this study, we explored the role of RBC-derived TG2 in thrombus formation using static *in vitro* models designed to mimic key features of RBC-rich clots typically observed in venous thrombosis.

2 | METHODS

2.1 | Blood samples and RBC isolation

Citrated venous blood was obtained from healthy volunteers after informed consent. This study was approved by the Medical Ethical Committee of Sanquin Research and was performed in accordance with the 2013 Declaration of Helsinki. The platelet-rich plasma was collected and stored at room temperature for 2 to 4 hours prior to use. RBCs were isolated by whole blood centrifugation (15 minutes, 210*g*). RBCs were washed in saline-adenine-glucose-mannitol buffer (150 mM NaCl, 1.25 mM adenine, 50 mM glucose, 29 mM mannitol, pH 5.6; Fresenius Kabi) and stored at 4 °C for a maximum of 4 hours before further processing.

2.2 | Preparation of clots

To allow treatment of RBCs with different inhibitors, reconstituted blood was used for inhibitor and knockout (KO) experiments. Two inhibitors with distinct properties were used. T101 (10 μM; Zedira) is a reversible, broad-spectrum TG inhibitor, including FXIIIa, which acts extracellularly due to its lack of membrane permeability. In contrast, Z-DON (80 μM; Zedira) is an irreversible, TG2-specific inhibitor that is membrane permeable and does not inhibit FXIIIa, even extracellularly. Isolated RBCs treated with either T101 or Z-DON for 30 minutes at 37 °C were handled differently before clot induction: T101-treated RBCs were not washed due to the reversible nature of the inhibitor, whereas Z-DON–treated RBCs were washed after treatment to remove any residual inhibitor. All incubations and washings steps were performed in $HEPES^+$ buffer, which is HEPES buffer (20 mM 4-[2-hydroxyethyl]-1-piperazineethanesulfonic acid [HEPES], 132 mM NaCl, 6 mM KCl, 1 mM $MgSO_4$, 1.2 mM K_2HPO_4; pH 7.4) supplemented with 5 g/L human albumin (Sanquin Plasma Products), 5.5 mM D-glucose and 1 mM $CaCl_2$. Clot formation was initiated by adding tissue factor (TF; Innovin; Siemens Healthineers) and $CaCl_2$ at final concentrations of 1 pM and 17 mM, respectively. In the phospholipid experiments, a phospholipid-TGT mix (0.1 mM; Rossix) was added to whole blood prior to clot formation.

2.3 | Generation of TG2 KO RBCs

Hematopoietic stem ($CD34^+$) cells were isolated from mobilized peripheral blood obtained from leukapheresis material after informed consent. $CD34^+$ cells were collected according to the guidelines of NetCord FACT (by the Sanquin Cord Blood bank, Netherlands). TG2 and CD45 KOs were generated, using CRISPR-Cas9, as previously reported by Verhagen et al. [24]. In short, synthetic crRNAs (IDT) were annealed to a synthetic scaffold RNA (tracrRNA; IDT) for 5 minutes at 95 °C; 50 μg *sp*Cas9-3xNLS (produced in house) [24] was added to the guide RNA and incubated for 15 minutes at room temperature. Cells were nucleofected in a homemade buffer (5 mM KCl, 15 mM $MgCl_2$, 120 mM Na_2HPO_4/NaH_2PO_4; pH 7.2, and 50 mM mannitol) [25]. Nucleofections were performed using a P4 nucleofector and 16-wells nucleofection strips (Lonza Bioscience). KO efficiency was determined by Western blot or flow cytometry. TG2 and CD45 KO cells were generated with the following guides: GTGCTGGGTCTTCGCCGCCG (TG2) and GAGGATCCTCAGGCACCCCG (CD45). CD45 is a protein expressed in early-stage RBCs but absent in mature reticulocytes, making this a suitable negative control. Erythroblast expansion and differentiation was performed as previously described [26]. Cultured RBCs (20×10^6) were used to form 5 μL clots by adding fresh human citrated plasma with TF (1 pM) and calcium ions (17 mM $CaCl_2$).

2.4 | Flow cytometry

Cells were harvested (200,000 cells/well) and washed in $HEPES^+$. Cells were incubated with an antibody mix containing CD235a-PE (0.1 μg/mL; BD Bioscience), CD71-VioBlue (1:200; MiltenyiBiotec), and DRAQ-5 (2.5 μM; Abcam) for 30 minutes at 4 °C. After washing, 10,000 events were recorded by flow cytometry (Canto II-F60 machine; BD Biosciences). Data analysis was performed with Flowjo 7.2.5 software (FlowJo v10; Tree Star).

2.5 | Phosphatidylserine detection

Isolated RBCs or cultured RBCs were stained with annexin V FITC (0.3 μg/mL; BD Biosciences) in $HEPES^+$ buffer containing 2.5 mM $CaCl_2$. Staining was performed for 30 minutes at 4 °C. EGTA (0.1 mM) was used as negative control for the annexin V staining. Flow cytometry was used to assess the binding of annexin V.

2.6 | Immunofluorescence staining of cells for microscopy

Antibody staining was performed for 30 minutes at 4 °C in $HEPES^+$ buffer. Vybrant DiD (2 μM; ThermoFisher) staining was done at 37 °C. In all experiments, 40 μg/mL Alexa488-labeled fibrinogen (ThermoFisher) was added to the samples.

2.7 | Confocal light microscopy

Three-dimensional (3D) images of blood clots were acquired with Leica TCS SP8 confocal microscope using a 63× objective. Confocal imaging was performed in 16-well chambers (Ibidi). Image resolution was set at 1024 × 1024 pixels, equivalent to a pixel size of 60.1 nm. Additionally, 1 μm interval was applied for the acquisition of Z-stack images. Live cell imaging was performed with the same microscope with resonant scanning at 37 °C, 5% CO_2.

2.8 | Scanning electron microscopy

Whole blood clots were formed as described previously. Samples were fixed for 24 hours in 2% glutaraldehyde solution (Sigma-Aldrich). The samples were rinsed in cacodylate buffer (150 mM sodium chloride, 50 mM cacodylate [Sigma-Aldrich]; pH 7.4), dehydrated in increasing concentration of ethanol (10%-100%), dried with hexamethyldisilane (Sigma-Aldrich), and sputter-coated with gold particles for 3 minutes. Some thrombi were cut prior to the sputter coating so that the interior could be imaged as well. Samples were imaged with a Helios NANOLAB 650 scanning electron microscope (FEI) at 10 kV. Unless indicated differently, all images were obtained with 46,000× magnification (pixel size, 6.7 nm), encompassing 6 randomly selected regions across 5 healthy donors.

2.9 | Extracellular vesicle isolation and analysis

RBC vesiculation was induced with 5 μM ionomycin (A23187; Sigma-Aldrich). RBCs were stimulated for 20 minutes at 37 °C in $HEPES^{+}$. Subsequently, RBC-derived extracellular vesicles (EVs) were isolated using multiple ultracentrifugation steps (300, 2000, 10,000, and 100,000 g) [27]. Samples were analyzed by calibrated flow cytometry (Apogee A60- Micro; Apogee Flow Systems, UK). Rosetta Calibration v2.04 (Exometry, The Netherlands) was used to link particle size to flow cytometry scatter signals, and MATLAB R2020b was used to determine their concentration [28].

2.10 | Tissue plasminogen activator–induced clot lysis

Clot lysis of contracted blood clots was initiated with 200 ng/mL of tissue plasminogen activator (tPA; Actilyse) from Boehringer Ingelheim Gmbh and imaged for 3 hours in $HEPES^{+}$ at 37 °C. RBCs were labeled with DiD (2 μM), and Alexa488-labeled fibrinogen was used to visualize fibrin in contracted clots. Confocal microscopy was used to follow clot lysis in real time.

2.11 | Quantification and statistical analysis

Both data representation and analysis were performed with Graphpad Prism 9.1.0 (221; Graphpad Software). The shown significances are derived from either unpaired *t*-tests or analysis of variance (ANOVA) analyses: ns = not significant or $P \geq .05$; $^{*}P \leq .05$; $^{**}P \leq .01$; $^{***}P \leq .001$; $^{****}P \leq .0001$.

2.12 | Additional methods

Additional methods can be found in the Supplemental Methods.

3 | RESULTS

3.1 | TG2 inhibition alters the structure of the fibrin network during clot contraction

Our study focused on understanding how RBC-derived TG2 influences the properties of RBCs in the context of clot formation, using 2 inhibitors with distinct properties to assess these effects. The following inhibitors were used: T101 (inhibits FXIIIa and other TG) and Z-DON (specific TG2 inhibitor). To confirm the specificity of Z-DON, FXIII activity was measured in normal human plasma in the presence or absence of T101 and Z-DON. FXIII activity was reduced by ∼92.8% upon T101 treatment, whereas Z-DON had no effect (Supplementary Figure 1). To assess Z-DON's cytotoxic effects, RBC deformability was analyzed. The results showed matching deformability profiles of Z-DON–treated samples and untreated controls (Supplementary Figure 2A), indicating no impact on RBC membrane integrity or flexibility. Additionally, critical deformability metrics (eg, EImax, Omin, and Ohyper) showed no difference between groups (Supplementary Figure 2B).

Blood clots formed in the presence of T101 retained fewer RBCs and the total weight of the thrombus was significantly reduced by 34% (Supplementary Figure 3) compared with the untreated clots, as was previously described [10,29]. On the surface of normal contracted clots, both fibrin and RBCs were present (Figure 1A, D). Large differences in clot structure were observed when T101 inhibitor was present during clot formation. The contracted clot was encapsulated by a dense layer of fibrin (Figure 1B, E) and the diameter of the fibrin fibers was decreased by 11% (Figure 1G). Additionally, clots that were formed in the presence of T101 mainly contained biconcave-shaped RBCs (75% ± 9%) in the center of the clot while polyhedron-shaped RBCs (41% ± 20%) were observed in control clots (Figure 2A and Supplementary Figure 4).

The presence of Z-DON resulted in clots with fewer and thinner fibrin fibers (Figure 1C, F) in the outer layers of the clot. Analysis of 3D images showed a significant decrease in both the fibrin density and fiber length (cumulative length of all fibrin fibers within the analyzed volume of the clot) at the surface of blood clots treated with Z-DON (Figure 1G), with a 1.5-fold and 1.8-fold reduction, respectively. Additionally, a larger average pore size was detected on the exterior of Z-DON–treated blood clots, indicating the formation of a less dense clot. Quantification of extruded RBCs, which is an indication of clot size, showed no differences between control and Z-DON–treated clots (Supplementary Figure 5). The fibrin diameter of Z-DON–treated clots on the exterior was 120 ± 6 nm, which is significantly less (1.3-fold) than that in untreated clots (diameter of 160 ± 10 nm; $P = <.0001$) (Figure 1G). As shown in Figure 2A, the scanning electron microscopy (SEM) images of the core of the clots revealed fibrin strands in the Z-DON–treated sample, while the untreated clots showed a less pronounced fibrin presence. Additionally, the SEM images also revealed that polyhedrocyte formation was unaffected in the sample treated with Z-DON. However, further examination of the fibrin network with confocal microscopy on thin

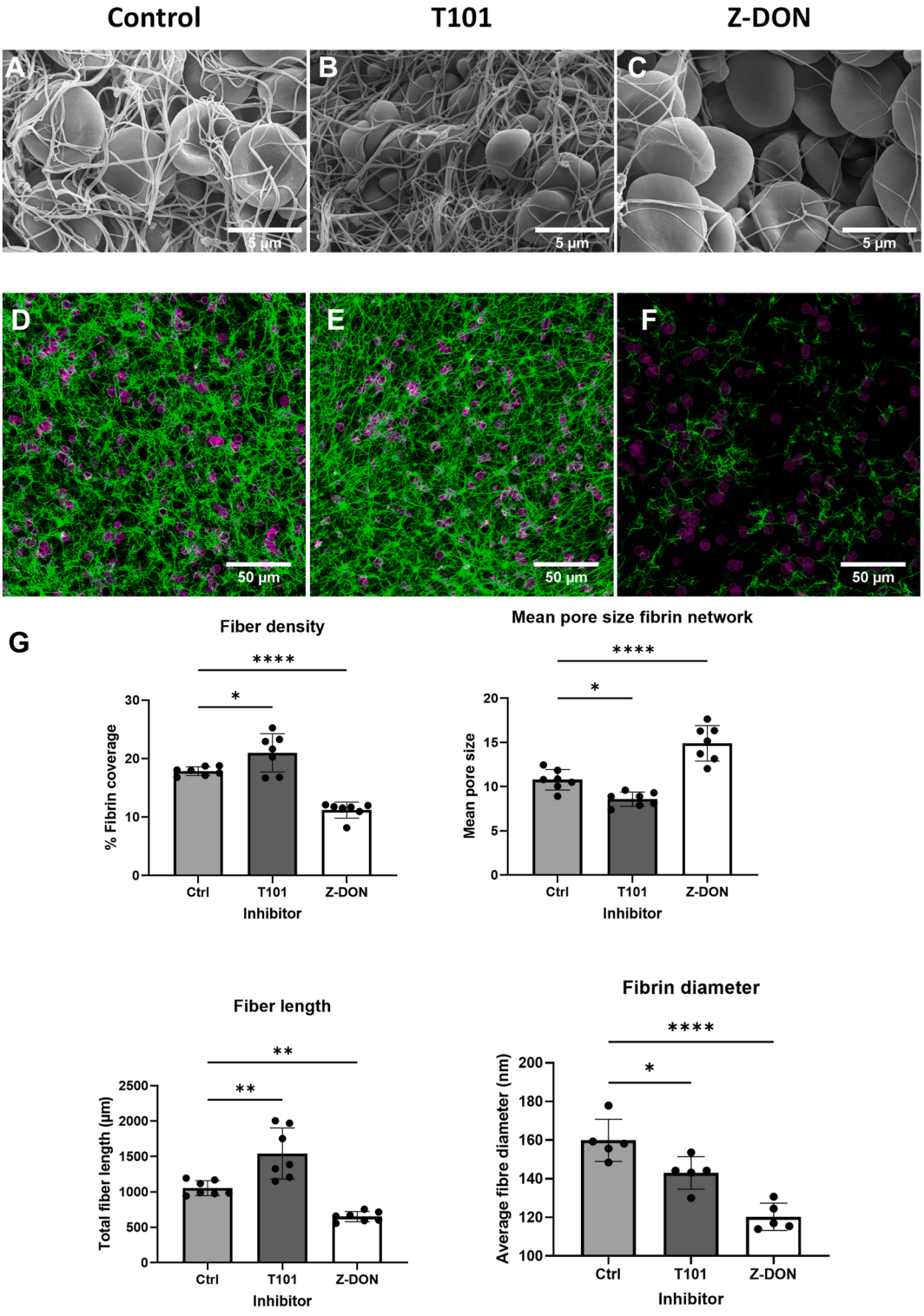

FIGURE 1 Effects of factor (F)XIIIa and transglutaminase (TG)2 inhibitors on blood clot structure. (A–C) scanning electron microscopy (SEM) images of the exterior (surface) of contracted blood clots that were formed in the absence (A) or presence of a FXIIIa inhibitor (T101) (B) or a TG2 inhibitor (Z-DON) (C). (D–F) Confocal images of the exterior of blood clots formed in the absence (D) or presence of T101 (E) or Z-DON (F). Z-stacks were generated with a standard Z-step size of 1 µm. Fibrin is depicted in green, and red blood cells are stained purple (CD235a Alexa647). (G) Quantification of fibrin properties from confocal images (7 healthy donors) and SEM images (5 healthy donors) using Fiji. For confocal images, the analysis included measurements of fibrin density, total fiber length, and mean pore size of the fibrin network. Fibrin diameter measurements were specifically performed on SEM images.

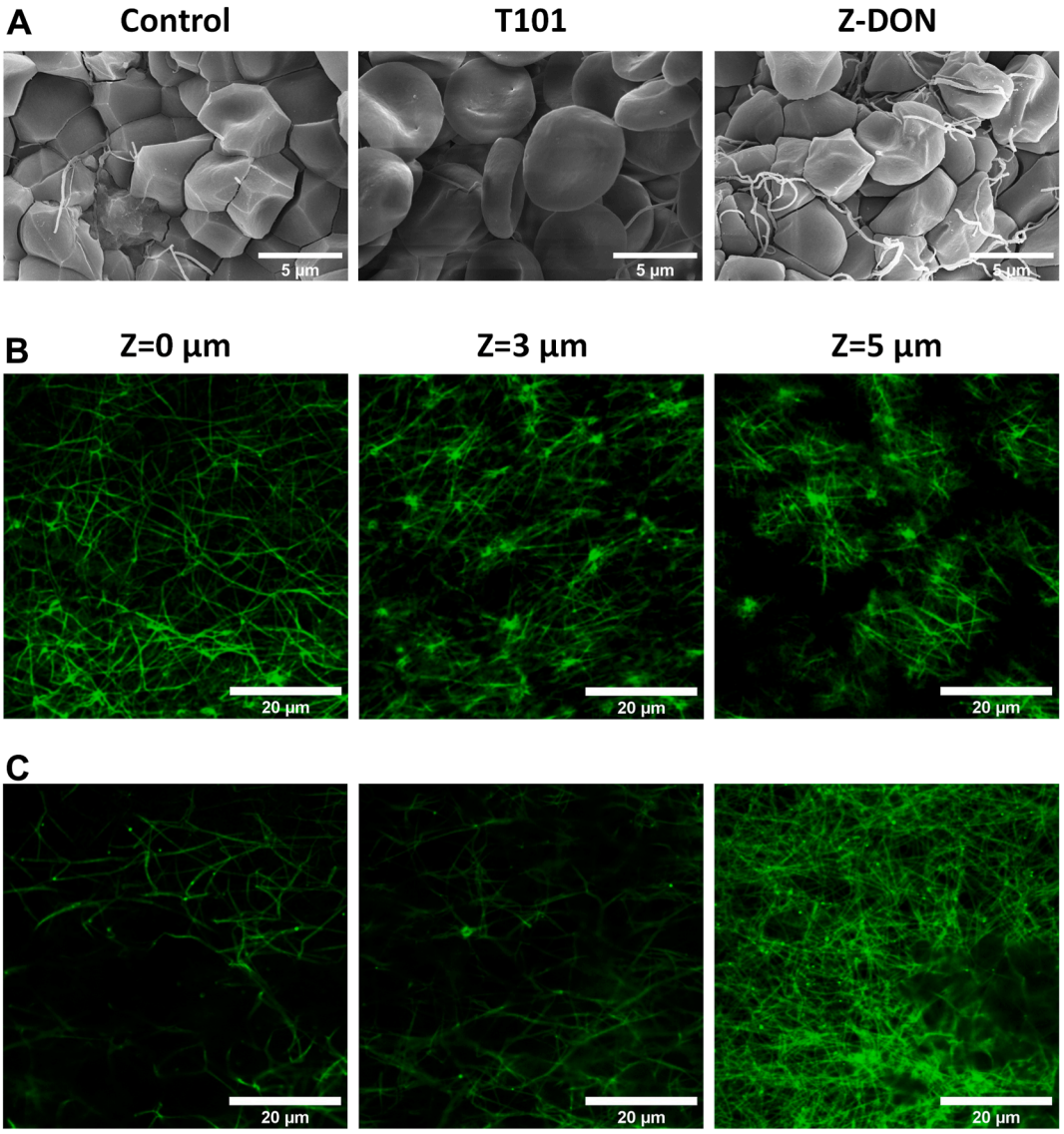

FIGURE 2 Visualization of fibrin localization. (A) Scanning electron microscopy (SEM) images of the central core region of whole blood clots. Data are representative of 5 independent experiments. (B, C) Thin whole blood clots between 2 coverslips imaged by confocal microscopy (Leica SP8; objective 63×). Z-stack projections of untreated blood clots (B) and Z-DON–treated blood clots (C) showing the heterogeneity of the fibrin network at 0, 3, and 5 µm distance from the glass slide. Alexa488-labeled fibrinogen was added to the clots to visualize the fibrin network. Data are representative of 3 healthy donors. (D) Quantification of fibrin diameter comparing clot surface and deeper regions in Z-DON–treated blood clots (n = 5). (E) A high-magnification image of a red blood cell interacting with the fibrin network (indicated by red arrows) in the absence (left image) or presence (right image) of Z-DON. Representative images of n = 5.

clots formed between 2 coverslips, which allowed more visualization beyond the surface, revealed a redistribution of fibrin away from the clot surface in Z-DON–treated clots (Figure 2B, C and Supplementary Figure 6), whereas untreated clots displayed a more heterogeneous fibrin distribution. In Z-DON–treated clots, the fibrin diameter at the edge (120 ± 6 nm) was significantly smaller than that in the central core region of the clot (184 ± 22 nm) (Figure 2D). Lastly, high-magnification SEM images indicated that fewer fibrin strands appeared to be associated with the RBCs in the presence of Z-DON than those in the control clot (Figure 2E).

3.2 | Generation and validation of TG2 KO cells

TG2 KO RBCs were generated from $CD34^+$ cells and the growth and differentiation process toward RBCs was evaluated. No differences were observed in the growth (Supplementary Figure 7) and differentiation between wildt-ype (WT) and TG2 KO RBCs. During differentiation, a decrease of CD71 and an increase of CD235a was observed, resulting in mature RBCs (Figure 3A, B). In addition, cytospins of both wild-type (WT) and TG2 KO cells showed similar phenotypes and indicated the presence of enucleated cells.

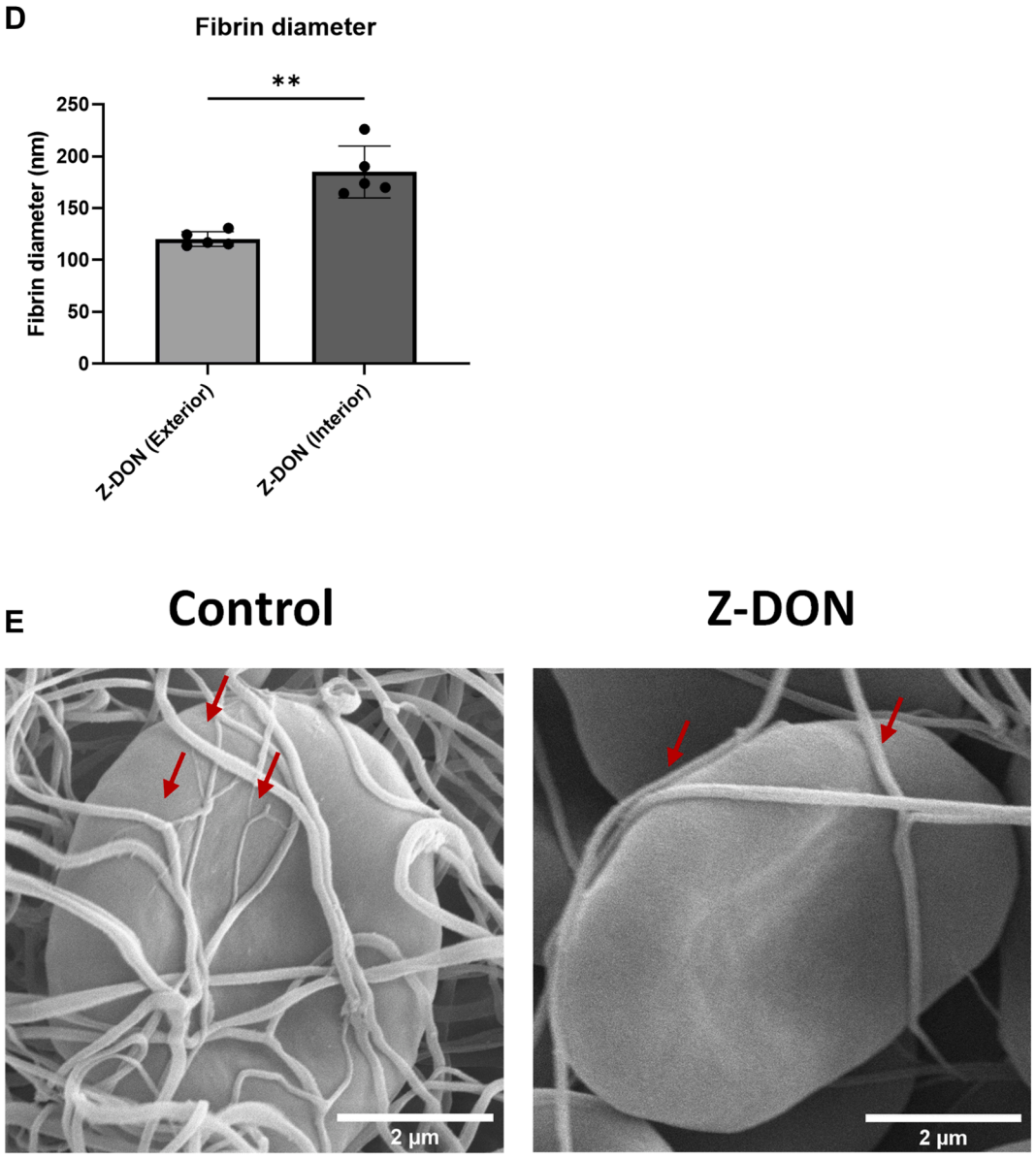

FIGURE 2 (*continued*).

TG2 expression in cultured RBCs was reduced to 5% of control levels (Figure 3C), and these TG2 KO RBCs were used to study the effect of TG2 on clot formation. In the absence of TG2 expression, a less dense fibrin network was observed on the exterior of the clots (Figure 3D, E), supporting the findings using the TG2 inhibitor (Figure 1C, F). To ensure that this effect was specific to TG2 knockout and not caused by the CRISPR editing process, a CRISPR control was included. Clots formed with CRISPR control RBCs displayed fibrin networks similar to those of WT RBCs, indicating that the changes in fibrin structure on the exterior was associated with the absence of TG2. Moreover, mixing TG2 KO RBCs with WT cells in different ratios resulted in a dose-dependent response of the fibrin density at the clot exterior region (Supplementary Figure 8). Using TG2 KO RBCs, our data demonstrate that the observed effects on fibrin structure at the surface during clot formation are specifically driven by RBC-derived TG2, rather than TG2 from other cell types.

3.3 | Effect of platelets on fibrin density in the presence of TG2 inhibition

During clot contraction, platelets generate the forces necessary to contract the clot and form an impermeable mass. To study the function of RBC-derived TG2 during clot contraction, clots were formed in the absence or presence of platelets.

A less dense fibrin meshwork was observed at the clot exterior when TG2 activity was inhibited, but only when platelets were present (Figure 4A, B and Supplementary Figure 9). In contrast, the fibrin

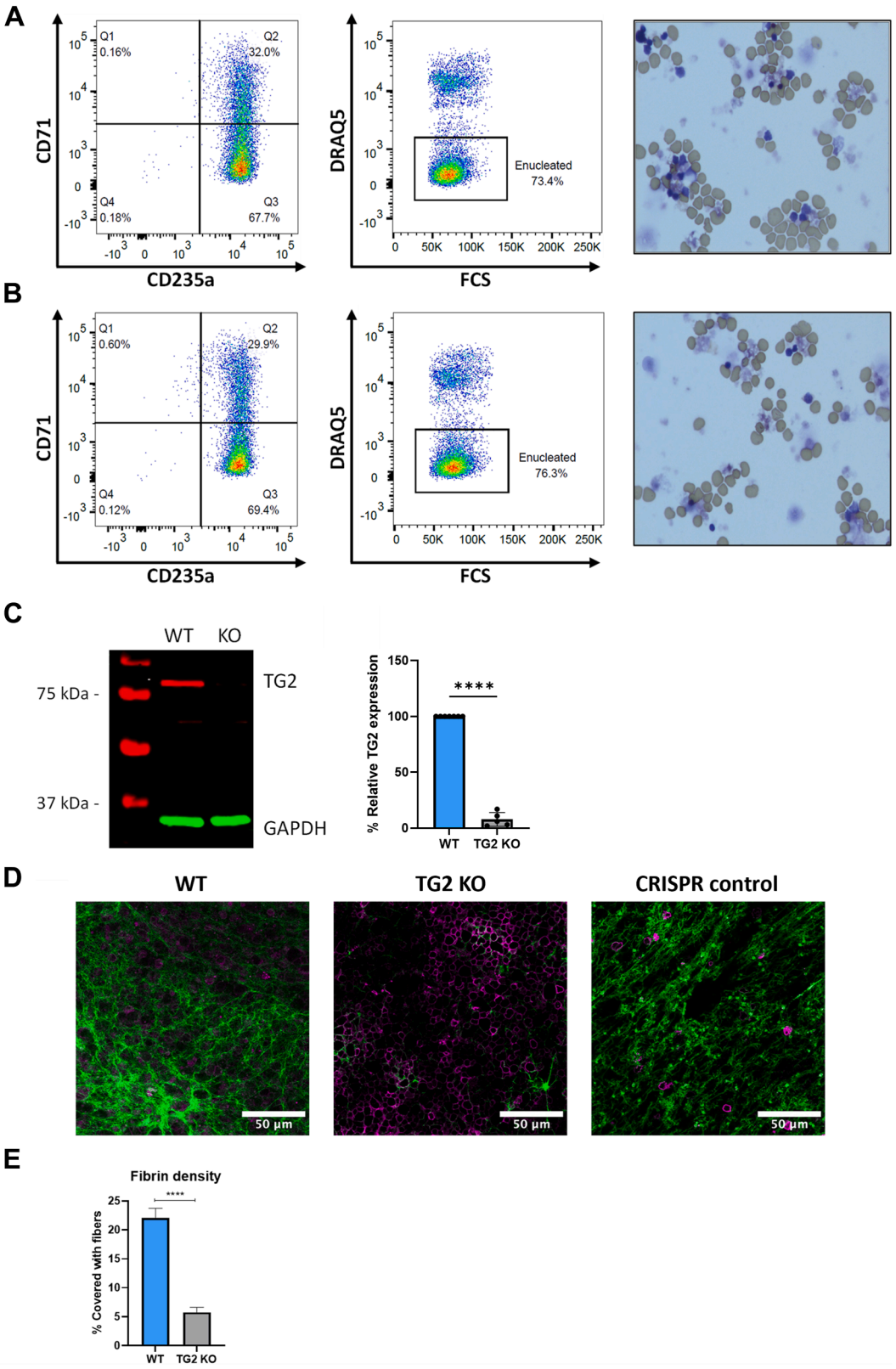

FIGURE 3 Expression of CD71/CD235a and DRAQ-5 at day 12 of erythroblast differentiation to determine the maturation and enucleation of (A) the wild-type (WT) cells and (B) the transglutaminase (TG)2 knockout (KO) cells. DRAQ-5 staining was used to indicate the presence of nuclei. Western blot was used to determine the KO efficiency of TG2 (indicated in red) and a loading control of GAPDH (in green) (C). (D) Confocal images of clot surfaces from TG2 KO (middle image), WT (left image), and CRISPR control (right image). Fibrin is stained with Alexa488 (green), while red blood cells (RBCs) were stained with CD235a Alexa647 (purple). (E) Quantification of fibrin density and area at the clot surface. In the absence of TG2 expression, the mean area of fibrin as well as the fibrin coverage were significantly reduced, resulting in a less dense fibrin network at the outer regions of the clot. Fibrin quantification of the confocal images was performed using Fiji. Data were collected from 4 different donors.

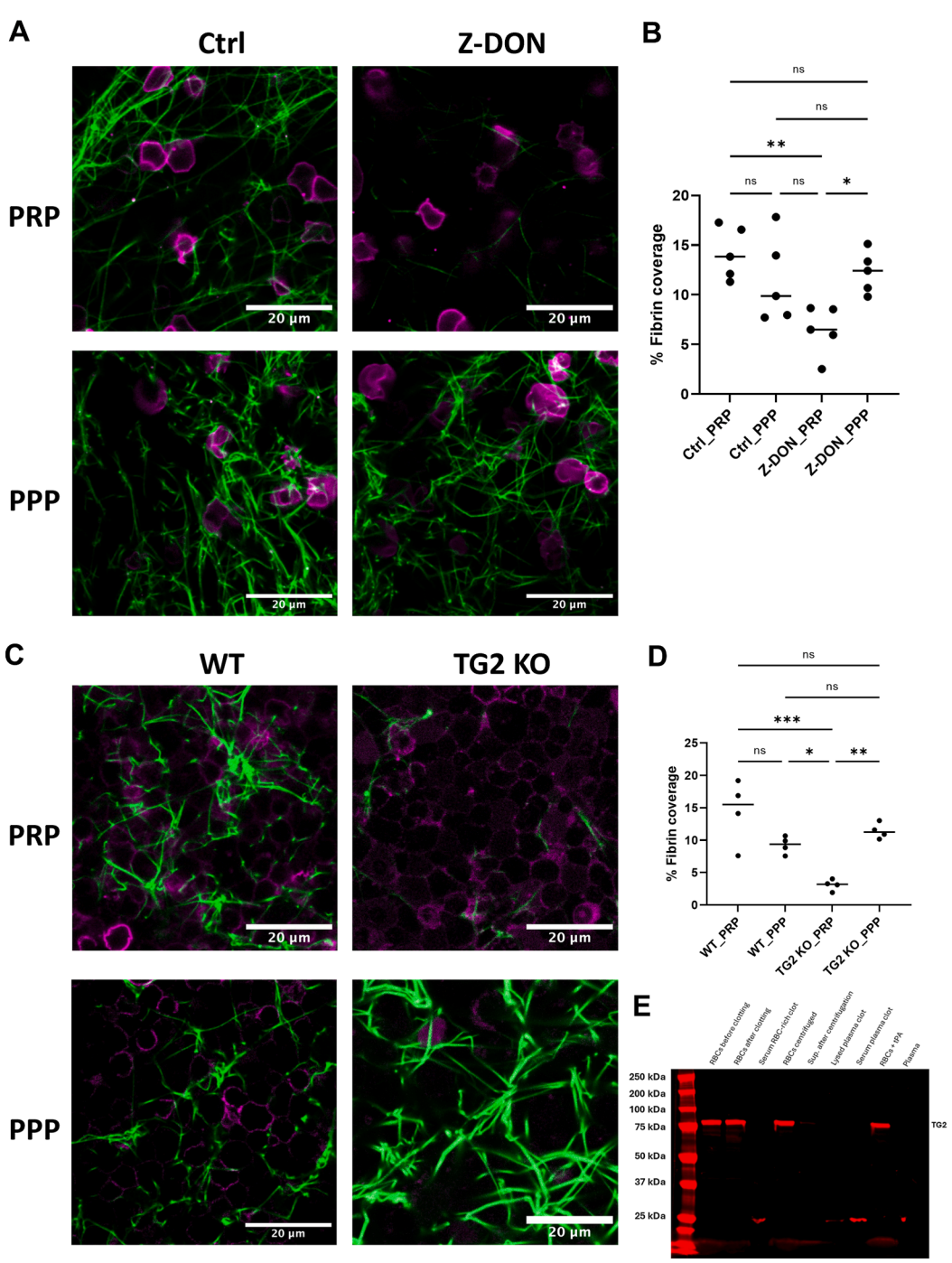

FIGURE 4 Fibrin density in clots in the absence or presence of platelets. (A) 3D confocal images of the surface of clots formed with (upper panels) and without platelets (lower panels), demonstrating that the Z-DON–induced reduction in fibrin density is only observed when platelets are present. Fibrin is depicted in green (stained with Alexa488-labeled fibrinogen) and red blood cells (RBCs) in purple (stained with DiD). Images were acquired from the external regions of the clots. Z-stacks were collected with a standard Z-step size of 1 µm. Data were collected from n = 5 donors, with 1 representative experiment shown. (B) Graph of fibrin density quantification from confocal images of the clots exterior formed with platelet-rich plasma or platelet-poor plasma in the absence or presence of Z-DON. (C) Confocal images of clots surface regions formed with transglutaminase (TG)2 KO RBCs in the presence (upper images) and absence (bottom images) of platelets. Images were acquired using a Leica SP8 confocal microscope with a 63× oil immersion objective, a standard Z-step size of 1 µm, and a pixel size of 60.1 nm. Scale bar, 20 µm. Data were collected from 4 donors, with 1 representative experiment shown. (D) Fibrin density quantification graph from clots formed with TG2 KO RBCs, comparing conditions with and without platelets. Data are shown as mean ± SD; ANOVA analyses were performed. Additional details on Z-stack acquisition and analysis are provided in the Supplementary Information. (E) TG2 release from RBCs under various conditions. Western blot analysis was performed to detect TG2 under different experimental conditions: RBCs before clotting, RBCs after clotting, and tissue plasminogen activator (tPA)-induced lysis, serum after clotting, RBCs subjected to centrifugation to mimic platelet forces, supernatant after centrifugation, plasma before clotting, plasma after clotting, and serum after plasma clot formation. Plasma samples were included as a baseline to detect TG2 originating from platelets. For conditions containing RBCs, 1 million

structure at the clot exterior of platelet-depleted samples was unaffected by TG2 inhibition with Z-DON (Figure 4A, B and Supplementary Figure 10). Comparable results were obtained using TG2 KO RBCs (Figure 4C, D). Collectively, these results may suggest that the mechanical forces exerted by platelets contribute to the effects of TG2 inhibition on fibrin localization within the clot.

Since platelets generate significant forces during clot contraction, it raises the possibility that these forces might induce the release of TG2 from RBCs, potentially allowing TG2 to act extracellularly and influence fibrin structure. Previous studies have demonstrated that TG2 can crosslink fibrin(ogen) extracellularly, independent of thrombin-mediated fibrin polymerization [30,31].

To test this hypothesis and determine whether TG2 is released from RBCs due to platelet-generated mechanical forces during clot contraction, we performed a Western blot analysis under various conditions, including RBCs before clotting, RBCs after clotting and tPA-induced lysis, serum after clotting, RBCs subjected to centrifugation to mimic platelet forces, supernatant after centrifugation, plasma before clotting, plasma after clotting, and serum after plasma clot formation (Figure 4E). Plasma samples were included to establish a baseline of TG2 levels originating from platelets. Our results revealed no detectable differences in TG2 expression on RBCs, after clot formation or simulated mechanical forces. Specifically, there was no reduction in TG2 expression on RBCs, which would suggest TG2 leakage, nor was substantial TG2 detected in the supernatants, serum, or plasma samples. These findings indicate that TG2 does not leak from RBCs during clot contraction and therefore does not exert extracellular effects under these conditions. Instead, the role of TG2 in modulating clot structure appears to be confined to its intracellular activity. Collectively, our findings suggest that TG2 inhibition impacts fibrin organization specifically in the presence of platelets, likely due to the interaction of platelet-mediated mechanical forces with TG2's role in RBC membrane stability.

3.4 | Effect of Z-DON on fibrin formation induced by different coagulation activators

Next, we studied the effect of Z-DON on the extrinsic and intrinsic coagulation pathways by inducing clot formation with different activators. The activators that were assessed included batroxobin, acting as a thrombin-like enzyme (2 nM), low (1 pM) and high (20 pM) concentrations of TF, and thrombin (5 nM). Fibrin structure was assessed at the clot surface by confocal microscopy. In contrast to the situation with a low concentration of TF (Figure 1), the absence of TG2 activity did not alter the fibrin structure induced by batroxabin, thrombin, or a high concentration of TF (Figure 5A, B).

3.5 | TG2 inhibition enhances thrombin generation and clot initiation

To further investigate the mechanistic basis for TG2 inhibition on clot formation, we performed TF-initiated thromboelastography (TEG) and whole blood thrombin generation assays (TGA) with Z-DON alone or combined with blocking antibodies against coagulation FVIII and FIX. Z-DON treatment alone resulted in an approximately 30% shorter reaction time in TEG (Figure 6A, B) and accelerated thrombin generation, reflected by a reduced lag time, increased peak, and increased velocity index in TGA (Figure 6D, F), indicating enhanced coagulation. When Z-DON was combined with anti-FVIII/FIX antibodies, clot formation still began earlier than with anti-FVIII/FIX alone (Figure 6A, C); the reaction time was reduced by 16%. Similarly, thrombin generation was also accelerated under antibody-treated conditions (Figure 6E, G). These findings suggest that the effect of Z-DON is not solely dependent on feedback loops involving these factors but rather occurs downstream of FVIII and FIX. Thrombolysis was similarly accelerated by anti-FVIII/FIX with or without Z-DON (Figure 6B, C). In contrast, no difference in clot initiation was observed in TEG when clots were initiated using 10 pM TF, indicating that the Z-DON effect is diminished under high coagulation initiation conditions (Supplementary Figure 11).

To further test whether TG2 directly influences thrombin generation via extracellular activity, we added recombinant human TG2 to whole blood TGA. This had no effect on lag time or peak thrombin generation compared with untreated controls, confirming that extracellular TG2 alone does not alter thrombin kinetics (Figure 6D–G). Consistent with this, Z-DON had no detectable effect on thrombin generation in pooled plasma lacking cellular components, supporting its cell-dependent mechanism of action (data not shown).

3.6 | Inhibition of TG2 activity alters RBC-derived EV formation

Next, we investigated whether RBC-derived TG2 affects the fibrin network via the formation of RBC-derived EVs. Adding phospholipids increased fibrin density in Z-DON–treated clots (Figure 7A, B). Second, the addition of freshly isolated RBC-derived EVs to the Z-DON–treated RBCs restored fibrin density to levels comparable with those of untreated clots (Figure 7A–C). Finally, the concentration and size of the RBC-derived EVs increased upon stimulation with the calcium ionophore ionomycin and further increased in the samples treated with Z-DON (Figure 7D, Supplementary Figure 12). The addition of Z-DON to unstimulated RBCs already showed a

RBCs were loaded per sample. The results showed no decrease in TG2 expression in RBCs after clot formation, simulated platelet forces, or clot lysis, and no detectable TG2 was observed in supernatants, serum, or plasma. These findings indicate that TG2 remains in RBCs and does not leak extracellularly during clot formation or dissolution.

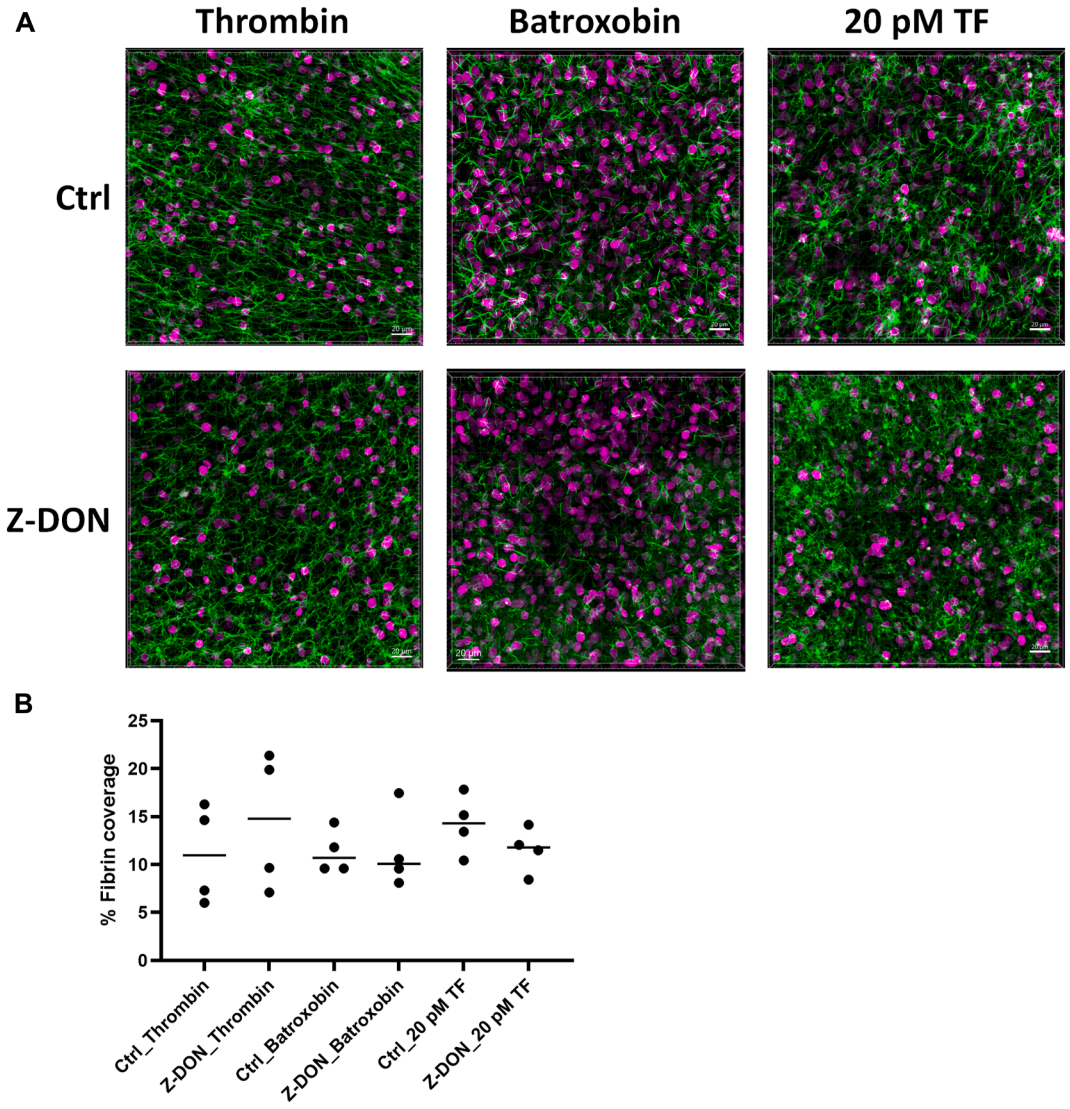

FIGURE 5 (A) 3D confocal images of the clot surface after activation with thrombin (5 nM), batroxobin (2 nM), and a high concentration (20 pM) of tissue factor (TF). The presence of Z-DON did not alter the structure of the fibrin network when initiated by thrombin, batroxobin, or high TF concentration. Fibrin is depicted in Alexa488, and red blood cells (RBCs) were labeled with DiD. Tile scan images were acquired using a Leica SP8 confocal microscope with a 63× oil objective and a standard Z-step size of 1 μm. (B) Fibrin quantification from confocal images of clot surfaces was performed using Fiji. Scale bar, 100 μm. Data are from 3 independent donors.

difference in EV formation compared with the untreated RBCs. Phosphatidylserine (PS) exposure on the RBC membrane was increased in RBCs treated with both ionomycin and Z-DON (Figure 7E). These findings were also supported by TG2 KO RBCs, which showed an increased exposure of PS when stimulated with ionomycin for 15 minutes (Figure 7F). Together, these data suggest that TG2 regulates vesiculation and PS exposure, which may underlie the accelerated thrombin generation observed with TG2 inhibition.

3.7 | TG2 plays a role in RBC membrane stability during clot lysis

The contribution of TG2 to the stability of the RBC membrane during thrombus dissolution is evident from the faster diffusion of DiD staining (a fluorescent marker for membranes) observed during live cell imaging in the presence of Z-DON (Supplementary Videos 1 and 2) compared with that of the untreated control. Quantification of DiD fluorescence intensity profiles over time demonstrated significantly faster diffusion in Z-DON–treated clots than untreated clots (Supplementary Figure 13), indicating compromised RBC membrane stability. In Z-DON–treated clots, DiD staining revealed large bright clusters that were absent in untreated clots, where the staining was uniform. These bright clusters likely represent aggregated membrane fragments or EVs, reflecting increased vesiculation and membrane destabilization due to TG2 inhibition. This aligns with TG2's role in reinforcing membrane integrity, where its inhibition leads to quicker membrane destabilization [24]. Our data do not indicate a loss of membrane integrity during the initial stages of clot formation or retraction, as no differences in DiD staining were observed after 3

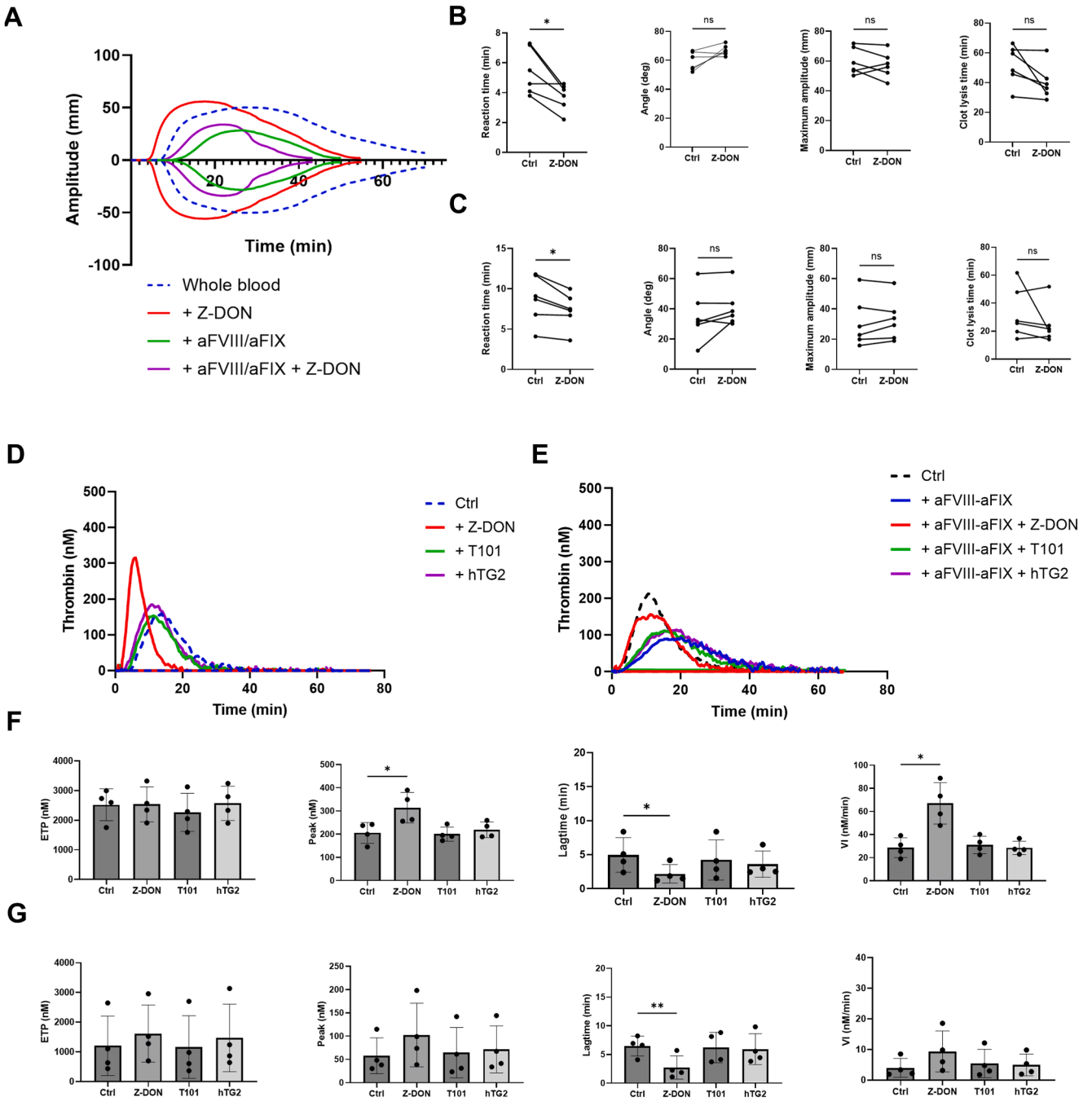

FIGURE 6 Transglutaminase (TG)2 inhibition enhances thrombin generation and clot formation in whole blood, even when factor (F)VIII/FIX activity is impaired. (A) Representative whole blood thromboelastography (TEG) treated with Z-DON (25 and 50 μM), anti-FVIII/FIX antibodies, or the combination of both, using 0.5 pM TF to initiate clotting. (B) Quantification of TEG parameters including reaction time (R), clotting angle, maximum amplitude (MA), and clot lysis time (CLT). (C) Quantification of TEG parameters in the presence of anti-FVIII/FIX antibodies. Z-DON significantly reduced reaction time compared with controls, both alone and with antibody treatment, indicating faster clot initiation. (D) Whole blood thrombin generation in the absence of anti-FVIII/FIX antibodies, showing enhanced thrombin generation with Z-DON. (E) Whole blood thrombin generation curve in the presence of anti-FVIII/FIX antibodies demonstrate that Z-DON retains its procoagulant effect under reduced intrinsic pathway amplification. (F) Quantification of whole blood thrombin generation parameters: endogenous thrombin potential (ETP), thrombin peak (nM), lag time, and velocity index (VI, nM/min) from D). (G) Quantification of whole blood thrombin generation parameters in the presence of anti-FVIII/FIX from panel (D). Data represent $n = 6$ for TEG and $n = 4$ for TGA.

hours of clot incubation across all conditions. This loss of staining is not due to photobleaching or a direct effect of Z-DON, as confirmed by imaging whole blood without clot formation and without tPA in both conditions, showing no dye diffusion. Furthermore, following thrombus dissolution, a higher count of so-called ghost RBCs (RBCs devoid of hemoglobin due to membrane rupture) was detected in

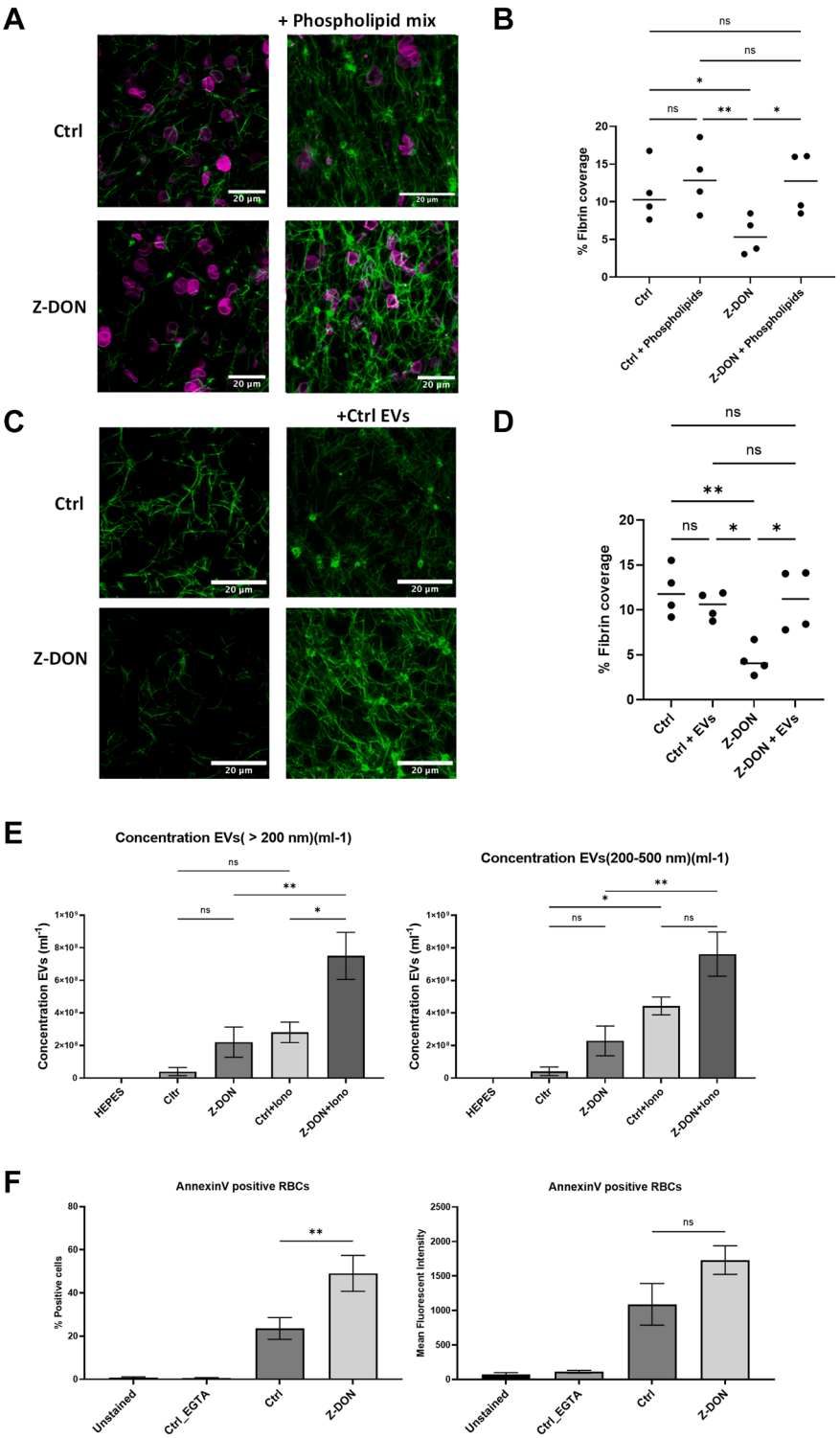

FIGURE 7 Effect of red blood cell (RBC)-derived EVs on clot formation. (A) Confocal images of whole blood clots supplemented with or without RBC-derived EVs and with or without Z-DON. A commercial phospholipid mix was evaluated. Both fibrin and RBCs were stained with Fbg-Alexa488 and DiD, respectively. (B) Fibrin quantification of the confocal images was performed using Fiji. A significant increase in fibrin density was observed upon phospholipid addition in Z-DON–treated clots, while no significant effect was observed in control clots. (C) Confocal images of whole blood treated with or without Z-DON and in the presence of RBC-derived EVs. Images were acquired with a Leica SP8 confocal microscope using a 63× oil objective and a standard Z-step size of 1 µm. (D, E) RBC-derived EVs were measured by microparticle flow cytometry (Apogee). RBCs were labeled with streptavidin-Alexa647 before ionomycin stimulation. Annexin V staining was performed to determine the phosphatidylserine (PS) exposure on EVs and RBCs. Data were collected from 6 donors. (F) Annexin V binding to PS on cultured RBCs and cultured transglutaminase (TG)2 KO RBCs after ionomycin incubation (15 minutes). The percentage of annexin V–positive cells is shown in the upper graph, and the mean fluorescent intensity (MFI) is shown in the lower graph. EGTA is used as a negative control for the annexin V staining. Data were collected from 5 donors.

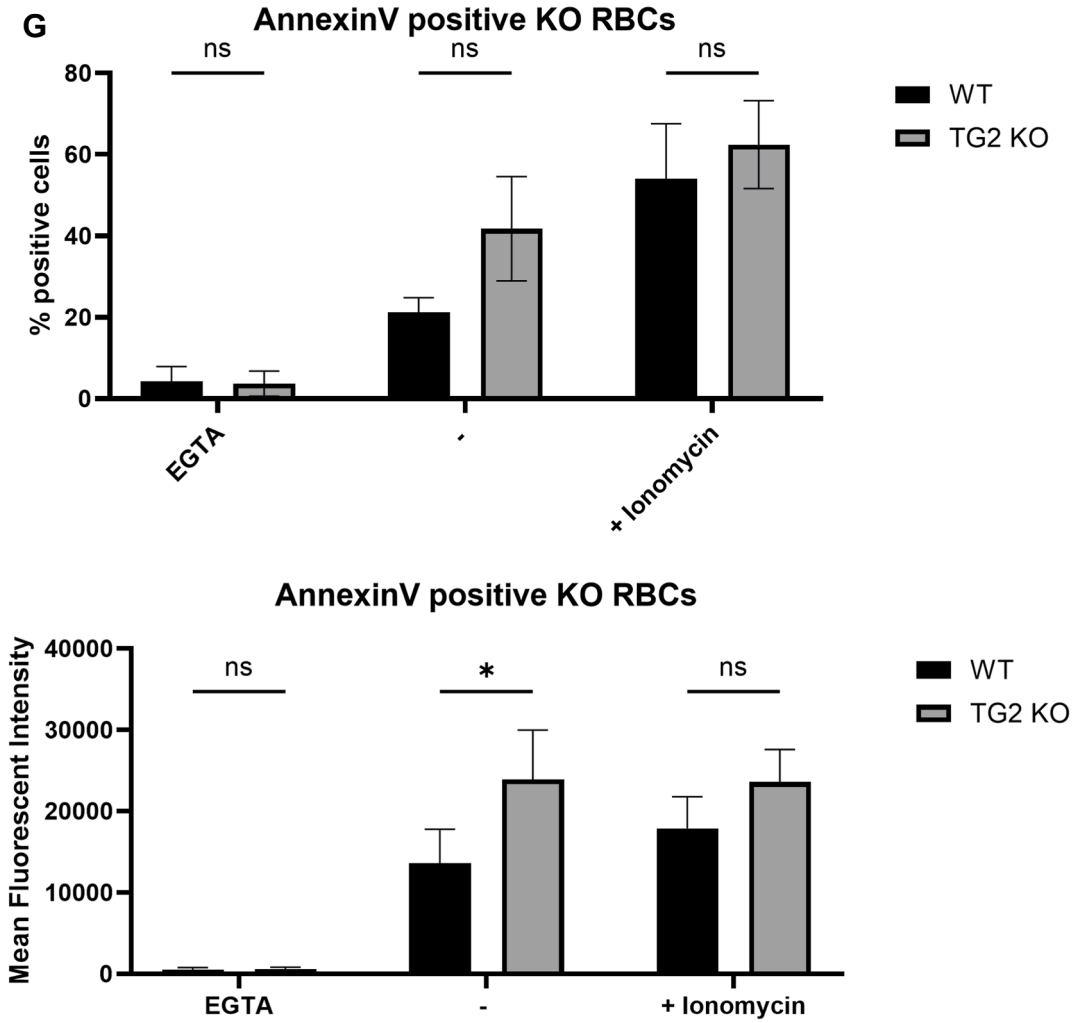

FIGURE 7 (*continued*).

samples treated with Z-DON, with these accounting for an average of 71% of the total RBC population observed, as shown in Figure 8. This, therefore, suggests that TG2 has a crucial function in preserving the integrity of the RBC cell membrane during clot lysis.

4 | DISCUSSION

Our study identifies a novel role for RBC-derived TG2 in clot formation, moving beyond the traditional view of RBCs as passive participants in coagulation. Several recent studies have challenged this outdated view, highlighting RBCs as active contributors to thrombosis through interactions with fibrin, platelet aggregates, and thrombin generation pathways [12,15,32,33]. The similarity in enzymatic activity between TG2 and FXIII provided the foundation for our investigations. While TG2 shares enzymatic properties with FXIII [23,34], our findings demonstrate that TG2 influences coagulation through mechanisms distinct from FXIII, particularly by modulating RBC membrane properties and vesiculation [23].

Using both pharmacological inhibition and genetic knockout of TG2, we demonstrated that RBC-derived TG2 significantly impacts fibrin architecture. Specifically, TG2-deficient clots exhibit fewer and thinner fibrin fibers at the exterior, accompanied by an internal redistribution of fibrin.

A key innovation of our study is the use of cultured RBCs from TG2 knockout progenitors to isolate the role of RBC-derived TG2, independent of other blood cell types. This approach enabled formation of small, well-controlled clots suitable for high-resolution analysis.

Mechanistically, our data suggest that TG2 indirectly regulates clot structure by modulating RBC-derived EV formation. In our experiments, TG2 inhibition increased vesiculation and PS exposure. These changes are expected to provide catalytic surfaces for thrombin generation, consistent with previous work showing that RBC-derived vesicles enhance coagulation [35,36] and that PS exposure provides catalytic surfaces for assembly of coagulation complexes [37]. Under stress conditions, TG2 becomes activated by elevated intracellular calcium and promotes crosslinking of

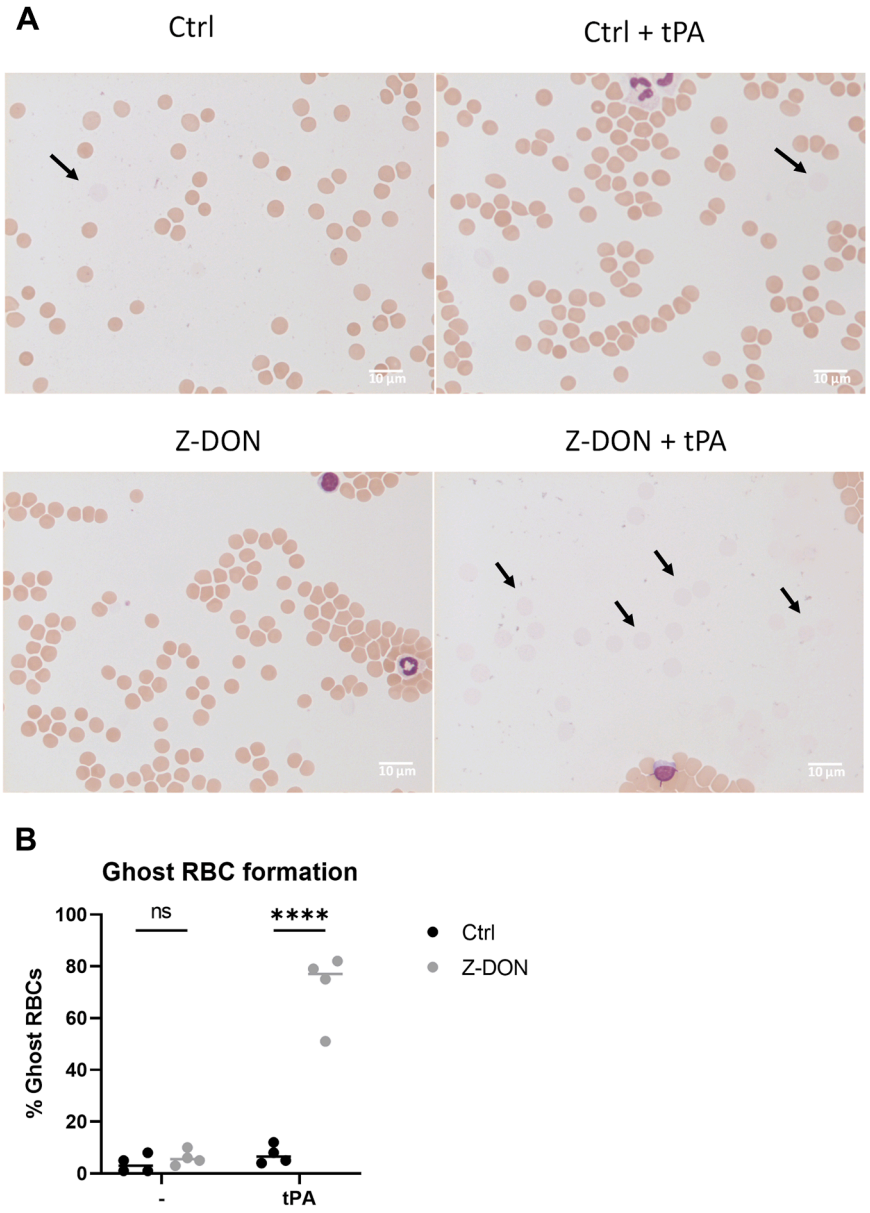

FIGURE 8 (A) Detection of ghost red blood cells (RBCs) after tPA-induced clot lysis by cytospin images. Cytospins were stained with May-Grünwald-Giemsa at an original magnification of 400×. Numerous ghost RBCs (indicated by black arrows) were evident on the cytospin. A dim staining was observed for the ghosts, indicating a loss of hemoglobin. (B) Quantification of ghost RBCs reveals 71% ghost RBCs in Z-DON–treated samples compared with those in controls, demonstrating a significant effect of Z-DON on RBC membrane integrity after clot lysis ($P < .0001$). Data are from 4 independent donors. Statistical significance: $P < .0001$.

cytoskeletal proteins such as spectrin and band 3, thereby stabilizing the membrane and suppressing PS externalization [23]. When TG2 is inhibited or absent, this regulatory mechanism is lost, resulting in increased PS exposure and EV release. These PS-positive RBCs and EVs act as procoagulant surfaces, supporting the assembly of tenase and prothrombinase complexes and thereby accelerating thrombin generation [15,33].

These findings are in line with evidence from sickle cell disease, where PS-positive RBCs correlate with thrombin generation markers such as prothrombin fragment 1.2 and D-dimers [16,35,38]. The procoagulant role of PS is attributed to its negative charge, which facilitates assembly of clotting factors [39]. Moreover, RBC-derived EVs in sickle cell disease promote thrombin generation through FXI-dependent mechanisms, supporting a PS-driven contribution to coagulation independent of tissue factor [35,40].

In line with this, whole blood TGA and TEG revealed accelerated thrombin generation and clot initiation upon TG2 inhibition using Z-DON. Z-DON accelerated coagulation even in the presence of anti-FVIII and anti-FIX neutralizing antibodies, indicating that TG2 acts independently or downstream of intrinsic pathway amplification loops. This supports a model where enhanced vesiculation compensates for reduced feedback activation in the coagulation cascade [15,36].

Providing further evidence for this mechanism, the addition of purified RBC-derived EVs or exogenous phospholipids partially restored fibrin density in Z-DON–treated clots, demonstrating that vesicles contribute functionally to clot structure. Conversely, recombinant TG2 added to whole blood did not alter thrombin generation, and we found no evidence that TG2 is released from RBCs during clot formation. These findings underscore that TG2's function

is intracellular and mediated via vesicle regulation, rather than through direct extracellular enzymatic activity.

TG2's effects are further amplified by platelet-driven mechanical forces. TG2 inhibition only altered fibrin structure in the presence of platelets, suggesting that platelets exacerbate the structural consequences of TG2 loss by intensifying membrane stress during clot contraction.

This interpretation is supported by studies showing that activated platelets compress RBCs into polyhedrocytes, increasing mechanical strain on the membrane [41,42]. This platelet-driven compression during clot contraction increases stress on RBC membranes, which makes TG2-mediated cytoskeletal crosslinking crucial for preserving membrane stability under these conditions.

These mechanical forces likely lead to uneven fibrin redistribution when TG2 is inhibited, as the loss of cytoskeletal anchoring disrupts fibrin organization. This is supported by our observation that in the absence of platelets, fibrin redistribution does not seem to occur. However, we found no evidence for TG2 release into the extracellular space under mechanical or enzymatic stress, reinforcing its role as an intracellular modulator.

Finally, we showed that TG2 contributes to RBC membrane stability during thrombolysis. Z-DON–treated clots exhibited increased ghost cell formation and rapid DiD diffusion from the RBC membranes, both indicative of membrane destabilization. These findings point to a role for TG2 in reinforcing the RBC membrane under lytic conditions, where its absence promotes vesiculation and potential clot fragility.

Taken together, our results reveal that RBC-derived TG2 regulates thrombus formation by stabilizing the RBC membrane, limiting vesiculation, and thereby influencing fibrin architecture and thrombin generation. In the absence of TG2, excessive EV formation and PS exposure provide catalytic surfaces that accelerate coagulation and alter clot structure. These findings position TG2 as a novel intracellular regulator of thrombosis and a potential therapeutic target in disorders characterized by aberrant clot formation.

ACKNOWLEDGMENTS

We thank Simon Tol, Mark Hoogenboezem, Erik Mul, Han Verhagen, and Dustin Laur for their invaluable technical support.

AUTHOR CONTRIBUTIONS

N.O.C. designed the experimental setup, performed experiments, designed figures, and wrote the manuscript; J.J.d.V. designed the analysis tool for fibrin quantification and performed confocal experiments. H.E. contributed with SEM imaging. C.H. and R.N. performed and consulted on the vesicle experiments with Apogee. H.L.M. and M.P.M.d.M. contributed with technological tools and provided insights into study design and interpretation of results. J.C.M.M. and R.v.B. designed the study, supervised the experiments, and wrote the manuscript. All authors read, revised, and approved the manuscript.

FUNDING

This work was funded in part by project grant 2019-02 from the Dutch Thrombosis Foundation.

RELATIONSHIP DISCLOSURE

J.C.M. is a consultant for Alveron Pharma and Synapse Research Institute.

DATA AVAILABILITY

Please contact Robin van Bruggen (r.vanbruggen@sanquin.nl) for data sharing.

ORCID

Naoual Ouazzani Chahdi https://orcid.org/0009-0004-7753-9087

REFERENCES

[1] Scridon A. Platelets and their role in hemostasis and thrombosis—from physiology to pathophysiology and therapeutic implications. *Int J Mol Sci*. 2022;23:12772.
[2] Weisel JW, Litvinov RI. Fibrin formation, structure and properties. *Subcell Biochem*. 2017;82:405–56.
[3] Lord ST. Molecular mechanisms affecting fibrin structure and stability. *Arterioscler Thromb Vasc Biol*. 2011;31:494–9.
[4] White RH. The epidemiology of venous thromboembolism. *Circulation*. 2003;107:I4–8.
[5] Wendelboe AM, Raskob GE. Global burden of thrombosis: epidemiologic aspects. *Circ Res*. 2016;118:1340–7.
[6] Bertina RM. Elevated clotting factor levels and venous thrombosis. *Pathophysiol Haemost Thromb*. 2003;33:395–400.
[7] Kuijpers MJ, Schulte V, Bergmeier W, Lindhout T, Brakebusch C, Offermanns S, et al. Complementary roles of glycoprotein VI and alpha2beta1 integrin in collagen-induced thrombus formation in flowing whole blood ex vivo. *FASEB J*. 2003;17:685–7.
[8] Tandon NN, Kralisz U, Jamieson GA. Identification of glycoprotein IV (CD36) as a primary receptor for platelet-collagen adhesion. *J Biol Chem*. 1989;264:7576–83.
[9] Ruggeri ZM, Mendolicchio GL. Adhesion mechanisms in platelet function. *Circ Res*. 2007;100:1673–85.
[10] Byrnes JR, Wang Y, Hansen CE, Ahn B, Mooberry MJ, Clark MA, et al. Factor XIIIa-dependent retention of red blood cells in clots is mediated by fibrin a-chain crosslinking. *Blood*. 2015;126:1940–9.
[11] van Gelder JM, Nair CH, Dhall DP. The significance of red cell surface area to the permeability of fibrin network. *Biorheology*. 1994;31:259–75.
[12] Byrnes JR, Wolberg AS. Red blood cells in thrombosis. *Blood*. 2017;130:1795–9.
[13] Ho CH. The hemostatic effect of packed red cell transfusion in patients with anemia. *Transfusion*. 1998;38:1011–4.
[14] Peyrou V, Lormeau JC, Herault JP, Gaich C, Pfliegger AM, Herbert JM. Contribution of erythrocytes to thrombin generation in whole blood. *Thromb Haemost*. 1999;81:400–6.
[15] Whelihan MF, Zachary V, Orfeo T, Mann KG. Prothrombin activation in blood coagulation: the erythrocyte contribution to thrombin generation. *Blood*. 2012;120:3837–45.
[16] Setty BY, Rao AK, Stuart MJ. Thrombophilia in sickle cell disease: the red cell connection. *Blood*. 2001;98:3228–33.
[17] Walton BL, Byrnes JR, Wolberg AS. Fibrinogen, red blood cells, and factor XIII in venous thrombosis. *J Thromb Haemost*. 2015;13:S208–15.

[18] Aleman MM, Walton BL, Byrnes JR, Wolberg AS. Fibrinogen and red blood cells in venous thrombosis. *Thromb Res*. 2014;133:S38–40.
[19] Lin SY, Chang YL, Yeh HC, Lin CL, Kao CH. Blood transfusion and risk of venous thromboembolism: a population-based cohort study. *Thromb Haemost*. 2020;120:156–67.
[20] Carson JL, Triulzi DJ, Ness PM. Indications for and adverse effects of red-cell transfusion. *N Engl J Med*. 2017;377:1261–72.
[21] Standeven KF, Carter AM, Grant PJ, Weisel JW, Chernysh I, Masova L, et al. Functional analysis of fibrin γ-chain cross-linking by activated factor XIII: determination of a cross-linking pattern that maximizes clot stiffness. *Blood*. 2007;110:902–7.
[22] Lorand L, Graham RM. Transglutaminases: crosslinking enzymes with pleiotropic functions. *Nat Rev Mol Cell Biol*. 2003;4:140–56.
[23] Sarang Z, Mádi A, Koy C, Varga S, Glocker MO, Ucker DS, et al. Tissue transglutaminase (TG2) facilitates phosphatidylserine exposure and calpain activity in calcium-induced death of erythrocytes. *Cell Death Differ*. 2007;14:1842–4.
[24] Verhagen HJ, Kuijk C, Rutgers L, Kokke AM, van der Meulen SA, van Mierlo G, et al. Optimized guide RNA selection improves *Streptococcus pyogenes* Cas9 gene editing of human hematopoietic stem and progenitor cells. *CRISPR J*. 2022;5:702–16.
[25] Bak RO, Dever DP, Porteus MH. CRISPR/Cas9 genome editing in human hematopoietic stem cells. *Nat Protoc*. 2018;13:358–76.
[26] Heshusius S, Heideveld E, Burger P, Thiel-Valkhof M, Sellink E, Varga E, et al. Large-scale in vitro production of red blood cells from human peripheral blood mononuclear cells. *Blood Adv*. 2019;3:3337–50.
[27] Yamashita T, Takahashi Y, Nishikawa M, Takakura Y. Effect of exosome isolation methods on physicochemical properties of exosomes and clearance of exosomes from the blood circulation. *Eur J Pharm Biopharm*. 2016;98:1–8.
[28] Hajji N, Hau CM, Nieuwland R, van der Pol E. Protocol for measuring concentrations of extracellular vesicles in human blood plasma with flow cytometry. In: Federico M, Ridolfi B, eds. *Extracellular vesicles in diagnosis and therapy. Methods in molecular biology*. 2504. New York: Humana; 2022:55–75.
[29] Aleman MM, Byrnes RJ, Wang JG, Tran R, Lam WA, Di Paola J, et al. Factor XIII activity mediates red blood cell retention in venous thrombi. *J Clin Invest*. 2014;124:3590–600.
[30] Murthy SN, Wilson J, Guy SL, Lorand L. Intramolecular crosslinking of monomeric fibrinogen by tissue transglutaminase. *Proc Natl Acad Sci U S A*. 1991;88:10601–4.
[31] Poole LG, Kopec AK, Flick MJ, Luyendyk JP. Cross-linking by tissue transglutaminase-2 alters fibrinogen-directed macrophage proinflammatory activity. *J Thromb Haemost*. 2022;20:1182–92.
[32] Faes C, Ilich A, Sotiaux A, Sparkenbaugh EM, Henderson MW, Buczek L, et al. Red blood cells modulate structure and dynamics of venous clot formation in sickle cell disease. *Blood*. 2019;133:2529–41.
[33] Sun S, Campello E, Zou J, Konings J, Huskens D, Wan J, et al. Crucial roles of red blood cells and platelets in whole blood thrombin generation. *Blood Adv*. 2023;7:6717–31.
[34] Ichinose A. Physiopathology and regulation of factor XIII. *Thromb Haemost*. 2001;86:57–65.
[35] van Beers EJ, Schaap MC, Berckmans RJ, Nieuwland R, Sturk A, van Doormaal FF, et al. Circulating erythrocyte-derived microparticles are associated with coagulation activation in sickle cell disease. *Haematologica*. 2009;94:1513.
[36] Tripisciano C, Weiss R, Eichhorn T, Spittler A, Heuser T, Fischer MB, et al. Different potential of extracellular vesicles to support thrombin generation: contributions of phosphatidylserine, tissue factor, and cellular origin. *Sci Rep*. 2017;7:6522.
[37] Zwaal RFA, Schroit AJ. Pathophysiologic implications of membrane phospholipid asymmetry in blood cells. *Blood*. 1997;89:1121–32.
[38] Setty BN, Kulkarni S, Rao AK, Stuart MJ. Fetal hemoglobin in sickle cell disease: relationship to erythrocyte phosphatidylserine exposure and coagulation activation. *Blood*. 2000;96:1119–24.
[39] Owens III AP, Mackman N. Microparticles in hemostasis and thrombosis. *Circ Res*. 2011;108:1284–97.
[40] van der Meijden PEJ, van Schilfgaarde M, van Oerle R, Renné T, ten Cate H, Spronk HMH. Platelet-and erythrocyte-derived microparticles trigger thrombin generation via factor XIIa. *J Thromb Haemost*. 2012;10:1355–62.
[41] Cines DB, Lebedeva T, Nagaswami C, Hayes V, Massefski W, Litvinov RI, et al. Clot contraction: compression of erythrocytes into tightly packed polyhedra and redistribution of platelets and fibrin. *Blood*. 2014;123:1596–603.
[42] Tutwiler V, Mukhitov AR, Peshkova AD, Le Minh G, Khismatullin RR, Vicksman J, et al. Shape changes of erythrocytes during blood clot contraction and the structure of polyhedrocytes. *Sci Rep*. 2018;8:17907.

SUPPLEMENTARY MATERIAL

The online version contains supplementary material available at https://doi.org/10.1016/j.rpth.2025.103274.